

Thin FRP/GFRC structural elements

G.B. Kim ^{a,*}, K. Pilakoutas ^b, P. Waldron ^b

^a Technology Advisory Division, Dongbu Corporation, Dongbu Financial Center 30F, Daechi-Dong, Gangnam-Gu, Seoul, 135-523, Korea

^b Department of Civil and Structural Engineering, The University of Sheffield, Mappin Building, Mappin Street, Sheffield S1 3JD, United Kingdom

Received 15 October 2005; received in revised form 22 March 2007; accepted 17 April 2007

Available online 6 May 2007

Abstract

This paper presents background work leading to the development of thin structural elements made of GFRC (Glass Fibre Reinforced Concrete) reinforced with FRP (Fiber Reinforced Polymer) bars. Such thin structural elements are suitable for a variety of applications such as cladding, security screens, etc, but this paper focuses on their use as permanent formwork. The first part of the paper deals with optimising a uniform thickness GFRC section to achieve maximum flexural capacity at minimum weight. The second part deals with the interaction between FRP and GFRC, in particular with the issues of bond. The third part presents the performance of a 3 m span thin GFRC permanent formwork panel system reinforced with FRP. Both experimental and analytical studies are presented and it is concluded that FRP/GFRC thin structural elements can be designed using conventional techniques requiring only the use of appropriate material characteristics.

© 2007 Elsevier Ltd. All rights reserved.

Keywords: FRP; GFRC; Thin structural elements; Permanent formwork; Bond stress–slip; Skin and rib design

1. Introduction

Innovative, economical and efficient methods of construction are continuously being sought by the construction industry. One particular area where there is still much scope for innovation is in the development of durable reinforced concrete (RC) thin structural elements. However, the problem with thin concrete structural elements is that, if unreinforced, they lack toughness and break easily during demoulding or transportation.

There are two main alternatives to solving this problem. The first is to use conventional steel reinforcement. However, an RC panel would then need to be at least 80 mm thick due to the requirement to provide cover for the steel for durability purposes. The second alternative is to employ GFRC (Glass Fibre Reinforced Concrete) using short fiber reinforcement such as Alkali Resistant glass fibres. This is already being used extensively in many non-structural architectural concrete applications with typical minimum

thicknesses of 20–50 mm in which the panel is usually supported frequently on a structural frame. A combination of the two alternatives is possible as demonstrated by the hybrid permanent formwork developed for the large drainage system shown in Fig. 1 which utilises the “skin and rib” design concept [1]. In this particular application, the formwork has a primary structural function for only a short period of time as the channel is backfilled with in situ concrete and, hence, there are no durability concerns. When durability is a bigger issue (such as for cladding panels or bridge permanent formwork) FRP reinforcement could be used as an alternative to conventional steel reinforcement.

This paper deals with the development of thin concrete permanent formwork. The first section introduces the main types of permanent formwork used today and discusses their advantages and disadvantages. Following that a thin GFRC section is considered and an optimisation exercise is undertaken to minimise weight for a particular span. This helps to identify the span and maximum length of an unreinforced thin GFRC element. Naturally, the next step is to reinforce the GFRC with FRP. Since no previous work has been done in this field the initial investigations deal with

* Corresponding author. Tel.: +82 2 34848697; fax: +82 2 34842356.
E-mail address: gbkim@dongbu.co.kr (G.B. Kim).

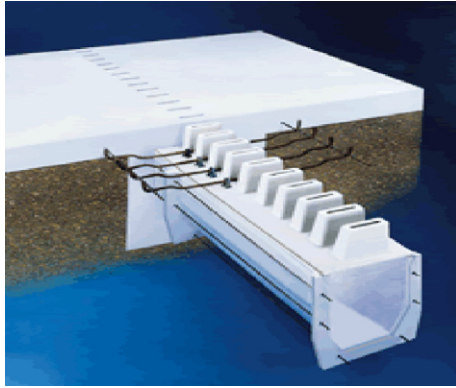


Fig. 1. GFRC drainage channel permanent formwork systems (Courtesy Hodkin & Jones Ltd., UK).

the bond characteristics. Finally, a thin FRP reinforced GFRC panel is tested and the paper presents the results and analysis.

2. Permanent formwork systems

Currently, the three most common materials used in permanent formwork systems are steel, precast concrete, and GFRC (Fig. 2). In the development of a new concept for permanent formwork, there are two major issues that need to be considered: (1) optimal utilisation of the material (cost constraint), and (2) achieving longer unsupported spans (technological constraint).

In the UK, steel decking is the most common permanent formwork system, especially for multi-storey steel framed building construction, because it is light and easy to install. Once in place, it requires very little additional connection to the frame and only small amounts of additional bar reinforcement. There are, however, a number of disadvantages with this system: (i) the profile of the decking is rolled from

a steel sheet of constant thickness, which does not necessarily lead to the optimal utilisation of the material; (ii) it spans in one direction only, which limits the unsupported span length; (iii) the steel is not placed in the optimal position so the strength of the steel is not fully utilised once composite action is established; and (iv) all steel structures must also be protected against fire which adds significantly to the cost if special finishes are required.

Precast concrete systems often offer an attractive and economic alternative to metal decking by eliminating the need for fireproofing and any additional finishes for durability. Nevertheless, due to the weight of such units, mechanised handling is generally required. In addition, a topping layer of concrete is needed to tie the concrete planks together. These can complicate and add cost to the installation.

The truss-plank type of formwork (Fig. 2c), which relies on a steel space truss partly embedded in a thin concrete slab, can span longer distances due to having an effective load carrying system in the form of a steel truss. This type of permanent formwork has potential economic advantages by providing speedy unpropped construction and excellent controlled surface finishes. However, due to the development of tensile strains induced in the precast concrete at the construction stage, the quality of the surface can be affected by unsightly cracking. Strong connections are also required between the top and bottom chords because shear strength is critical at the supports.

Thin-walled GFRC is already commonly used for a range of small elements like channels, ducts and cladding panels, and, due to its light weight, has considerable potential in the development of new permanent formwork solutions. However, in order to deliver deflection control during construction, the overall depth of unsupported GFRC formwork would have to be increased because the stiffness of GFRC is not as high as that of steel.

Although the permanent formwork solutions mentioned above are relatively efficient in their use of materials, the basic cost of materials could be reduced further by introducing a new philosophy for design and optimisation. By adopting new materials, such as FRP and GFRC, it is possible to design new systems for permanent formwork for particular applications in the construction market. The first part of this paper deals with section optimisation issues.

3. Optimum cross-section for a thin element as permanent formwork

The cost of permanent formwork is dominated by the amount of material used in its manufacture. As conventional metal decking is invariably made from steel sheet of constant thickness, the amount of material used is proportional to the total width of the strip from which it is formed. Fig. 3 shows cross-sections and dimensions of typical profiles in common use.

In the following calculations, it is assumed that sections behave as normal thin-walled beams. To reduce

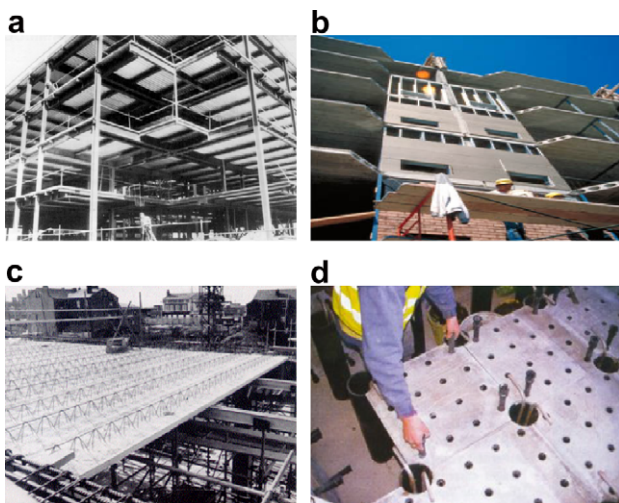


Fig. 2. Existing permanent formwork systems: (a) steel decking, (b) precast concrete hollow slabs, (c) pre-cast (truss-plank), (d) GFRC.

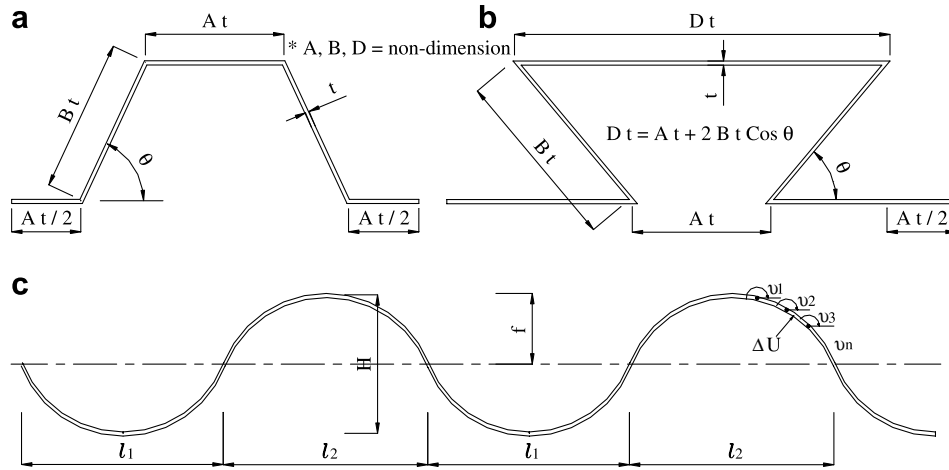


Fig. 3. The dimensions of single profiles from typical sections: (a) trapezoidal section, (b) re-entrant section, (c) sinusoidal section.

deflections in the formwork, the second moment of area of the section should be as large as possible. The second moment of area, I , and the weight of material per unit area, W_{ua} , of the trapezoidal section shown in Fig. 3a, are calculated using the formula given by Rockey and Evans [2]:

$$I = \frac{At^4}{6} + \frac{At^4}{2} [B \sin \theta - 1]^2 + \frac{t^4 B^3 \sin^2 \theta}{6} \quad (1)$$

and

$$W_{ua} = \frac{(A+B)\rho t}{(A+B \cos \theta)} \quad (2)$$

where ρ is the density of the sheet material. The section modulus per unit weight of a given section is given by

$$Z'_w = (I/y_m)/W_{ua} \quad (3)$$

where y_m is the distance from the bottom fibre to the neutral axis of the section.

The formulae in Eqs. (1)–(3) do not consider the possibility of buckling and are limited to an equal length of top and bottom plate. Because it is difficult to calculate the moment of inertia for any arbitrary cross-section, previous research by Timoshenko [3], Hopkins [4], Lee et al. [5], Chung [6], and Rajendran [7], has concentrated on standard approaches using the summation method to evaluate the general section properties. In order to investigate section properties of more complicated shapes, and in particular re-entrant sections, Eqs. (1)–(3) were modified by using an approximate method where the section is first discretized into a number of equal length segments. The moment of inertia for the sections shown in Fig. 3b and c, were calculated using Eq. (4) modified by the authors for re-entrant sections and Eqs. (5) and (7) proposed by Lee et al. [5] for sinusoidal sections

$$I = \frac{Dt^4}{6} + \frac{Dt^4}{2} [B \sin \theta - 1]^2 + \frac{t^4 B^3 \sin^2 \theta}{6} + B^3 t^4 \sin^2 \theta \cos \theta \quad (4)$$

$$I_x = \sum_{n=1}^m \Delta I_{xn} \quad (5)$$

$$\Delta I_{xn} = \frac{t_c (\Delta u)^3}{12} \sin^2 \theta_n + t_c (\Delta u) \bar{y}^2 \quad (6)$$

$$\bar{y} = \frac{y_n + y_{n+1}}{2} \quad (7)$$

where m is the total number of segments; Δu is the constant segment length; and ΔI_{xn} is the moment of inertia of a segment above the centroidal axis.

After comparing 16 different cross-sectional configurations having uniform thickness (see Fig. 4 and Table 1), the sinusoidal sections were shown to be the least efficient in terms of the moment of inertia per metre width, I'_m , followed by the trapezoidal sections. The optimum solution is given by the re-entrant section which is almost twice as efficient as the sinusoidal section. An additional and consequential problem of the sinusoidal sections is that they are less able to control deflections.

Fig. 5 shows the deflections and capacity of 10 mm thick GFRP sections with a constant overall depth of 110 mm. A load of 5 kN/m², including construction load and self weight of the wet concrete, was assumed when deriving deflections and load capacity. The sections are numbered in the same way as in Table 1. It can be seen that some of these sections would require support at centres less than 2.5 m if the maximum deflection at the construction stage is to be maintained at less than 1/500 (=0.002) of the span between props.

It can be concluded that GFRP sections of uniform thickness can be used as permanent formwork for moderate depths and spans, but will be limited in their range of

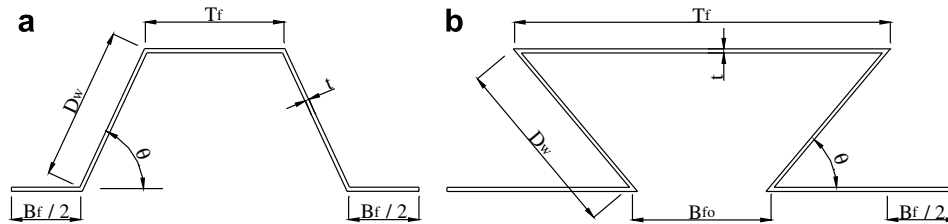


Fig. 4. Definition of profile variable: (a) trapezoidal section, (b) re-entrant section.

Table 1
Properties of different cross-sections for depth 100 mm, $t = 10$ mm

No.	θ°	$R = D_w/T_f$	$K = B_f/T_f$	$P = B_{fo}/T_f$	I (cm ⁴)	I'_m (cm ⁴ /m)	Shape
1	90	1.0	1.0	1.0	670	3354	
2	–	($l_1 = 1.0$)	($l_2 = 1.0$)	–	383	1916	
3	90	1.0	1.6	1.0	815	3135	
4	–	($l_1 = 1.0$)	($l_2 = 1.6$)	–	447	1720	
5	90	5.0	5.0	1.0	444	3704	
6	–	($l_1 = 0.2$)	($l_2 = 1.0$)	–	380	3173	
7	90	1.0	0.2	1.0	444	3704	
8	–	($l_1 = 0.2$)	($l_2 = 1.0$)	–	380	3173	
9	65	1.103	1.0	1.93	672	2294	
10	–	($l_1 = 1.1$)	($l_2 = 1.0$)	–	488	1666	
11	65	1.103	1.6	1.93	811	2295	
12	–	($l_1 = 1.1$)	($l_2 = 1.6$)	–	553	1565	
13	50	0.5	0.37	0.37	1518	4126	
14	(as 13 – rounded corners)				1416	3849	
15	50	0.5	0.6	0.37	1672	3906	
16	(as 15 – rounded corners)				1580	3691	

applications by deflection and capacity. Clearly, to increase the unsupported span, GFRP sections will need to be reinforced.

4. Proposal for new elements made of FRP reinforced GFRP

To avoid problems of durability associated with steel rebars with little cover, thin GFRP sections can be reinforced with FRP. This section examines the use of FRP reinforcement in thin GFRP sections designed using the “skin and rib” approach [1].

There are several issues to consider when dealing with FRP in GFRP sections: (i) the thickness of GFRP need not be constant; (ii) for practical purposes, the minimum thickness of GFRP has to be at least 5 mm; and (iii) the controlling stress in GFRP is its tensile strength since the compressive strength is much higher. Therefore, the FRP reinforcement should be added to the tensile region and the amount of GFRP below the neutral axis depth should be minimized to reduce weight. Two suitable sections proven by the authors in a more extensive study [8] to be best in terms of deflection control and capacity, respectively, are shown in Fig. 6.

The main design issues concerning the development of such permanent formwork include:

- (1) *Bond*. No previous studies have been reported on the interaction between GFRP and FRP, hence a comprehensive understanding of this interaction is required before the concept is accepted for further investigation.
- (2) *Cover*. GFRP is a good material for protecting reinforcement from the environment and FRP reinforcement does not require the same level of protection as conventional steel. Hence, the cover requirement can be relaxed provided that bond requirements can be met.
- (3) *Deflections*. Since GFRP is not that much stiffer than GFRP, it is necessary to increase the overall depth of its section to deliver better deflection control. Alternatively, the element will need to be pre-cambered, to counter some of the permanent deflection.
- (4) *Crack widths*. The crack width limit used in bridge structures, required for the protection of steel reinforcement, is normally less than 0.1 mm. In the case of FRP reinforcement this limit may be relaxed up to 0.5 mm as recommended by ACI 440.1R-01 [9].

5. Experimental programme

In designing reinforced concrete members, it is assumed that no slippage will occur between the bar reinforcement and the concrete when load is applied. If the bond capacity

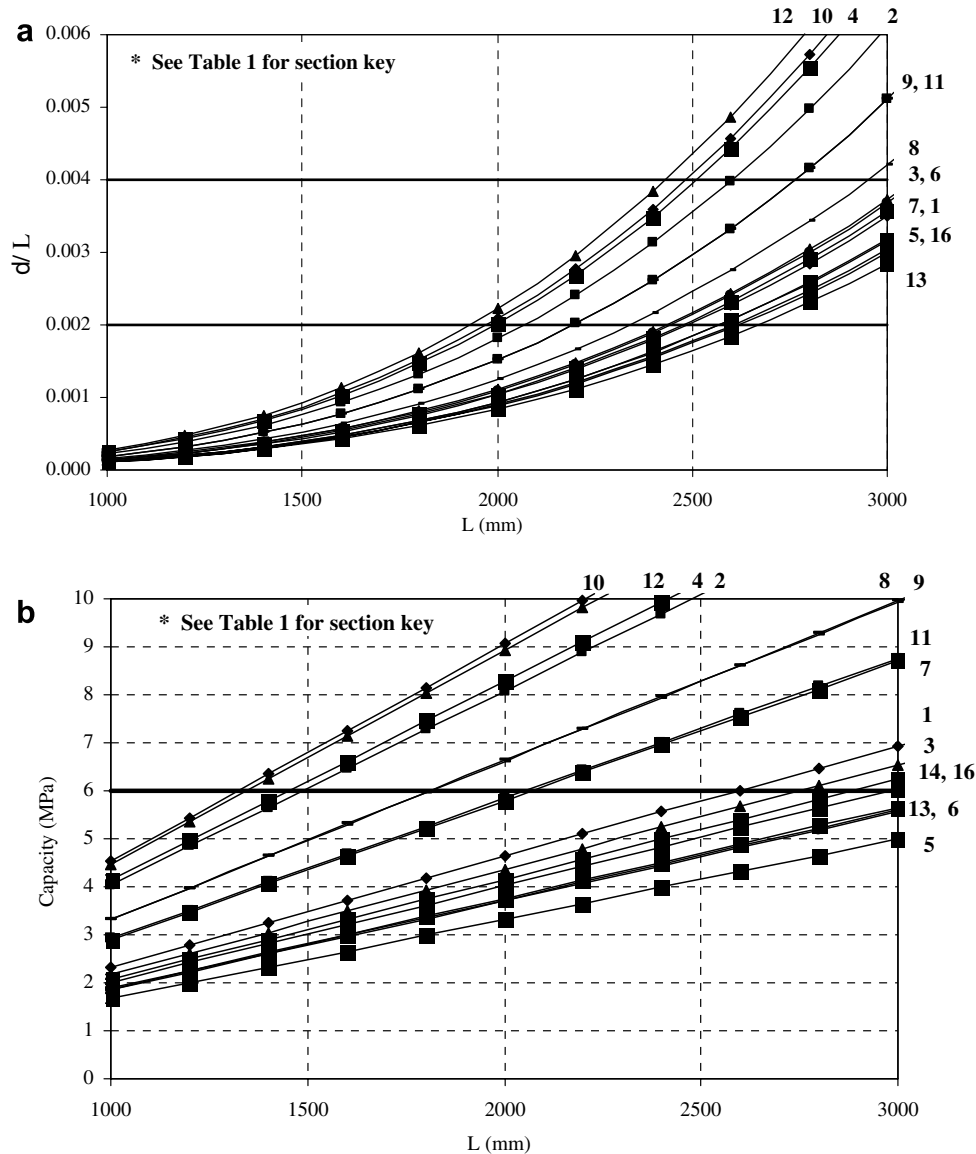


Fig. 5. Deflections and capacity for GFRC sections, $t = 10$ mm: (a) deflections vs. span length (see also Table 1 for section key), (b) capacity vs. span length (see also Table 1 for section key).

between the two is exceeded, the concrete surrounding the reinforcement may crush or split permitting the embedded bar to slip. The strength of reinforcing bar-to-concrete bond is dependent upon a number of factors, with concrete compressive strength, reinforcing bar diameter and spacing, and embedment length being the most significant. Nominal bond strength is determined experimentally by the pull-out test, which basically involves measuring the force needed to produce measurable slippage or pull out of a bar embedded in concrete.

The experimental work on bond deals with both direct pull-out tests and splitting pull-out tests. Standard pull-out tests are needed to determine the bond characteristics in well confined conditions, whilst the splitting pull-out tests enable us to understand better the bond behaviour in thin flexural elements.

5.1. Manufacture of pull-out specimen

The GFRC was made from Type I Portland cement, sand, and chopped glass fibres of 15 mm maximum length. Mix 1 and Mix 2 were designed with different volume fractions of fibres of 2% and 3%, respectively. The mix proportions were 0.35:1.0:1.0 (water:cement:sand) by weight. Concrete test cylinders 100 dia \times 200 mm (six for each GFRC mix) provided average compressive strengths, f'_c of 54 MPa (Mix 2–24 days) and 66 MPa (Mix 1–40 days), respectively. The average tensile strengths at the same age were determined to be 6 and 7 MPa, respectively, by using the Brazilian test on three additional cylinders. Each pull-out specimen was cast with either 8 mm square Glass Fibre Reinforced Polymer (GFRP) bar, supplied by Eurocrete Ltd., ($E = 41$ GPa, strength = 900 MPa) having a rough

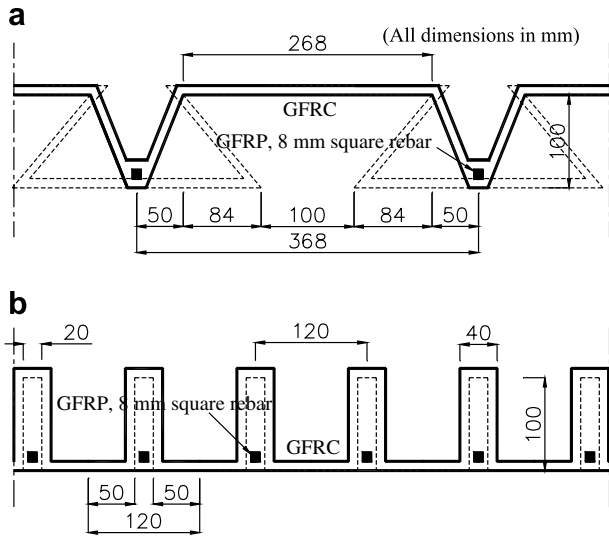


Fig. 6. FRP reinforced GFRC panels: (a) modified section Type M13, (b) modified section Type M5.

surface provided by a peel ply or 6 mm diameter (460 MPa) deformed steel bar. The position of the bars, embedment length and cover dimensions are shown in Fig. 8. After casting, specimens were cured in 100% humidity at ambient laboratory temperature for 24 or 40 days prior to testing.

5.2. Test specimens, variables and procedures

The characteristics of the local bond stress–slip response of reinforcing bars in GFRC were investigated by conducting 18 standard pull-out tests and 18 splitting pull-out tests based on the international Round Robin Test (iRRT) [10] procedure for FRP bars in normal unreinforced concrete.

Three specimens from each group were tested using a 500 kN capacity universal testing machine. Slip measurements were made using linear variable differential transducers (LVDTs) fixed on the surface of the cubes at both the loaded and free ends. Measurements of load and displacement were taken every 2 seconds by a computer controlled data acquisition system. Fig. 7 shows details of the positioning of the bar in the concrete cube and loading frame for both the standard pull-out and splitting pull-out tests. A schematic representation of the test setup, giving relevant dimensions, is shown in Fig. 8.

5.3. Standard pull-out tests

In the pull-out tests, the actual slip of the bar with respect to the concrete, δ_{le} , was calculated by subtracting the elastic elongation of the unbonded portion of the bar, Δl , from the average slip measurements of three LVDTs, δ_{av} , as shown in the following equations:

$$\delta_{av} = (\delta_1 + \delta_2 + \delta_3)/3 = \delta_{le} + \Delta l \quad (8)$$

$$\Delta l = Fl_a/(EA) \quad (9)$$

$$\delta_{le} = \delta_{av} - \Delta l = (\delta_1 + \delta_2 + \delta_3)/3 - Fl_a/(EA) \quad (10)$$

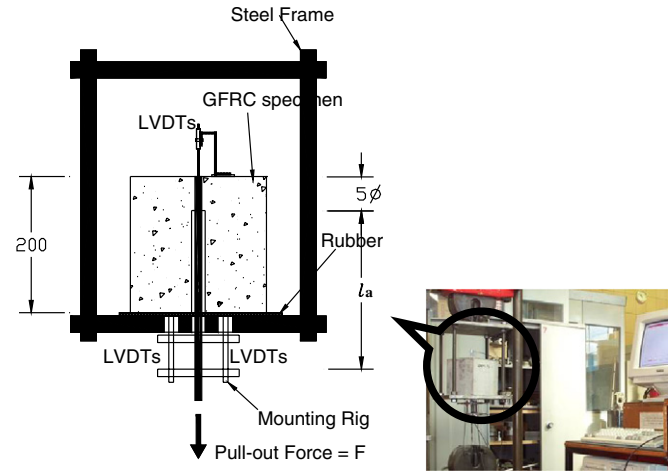


Fig. 7. Details of the positioning of the bar and LVDT's in the GFRC specimen and loading frame.

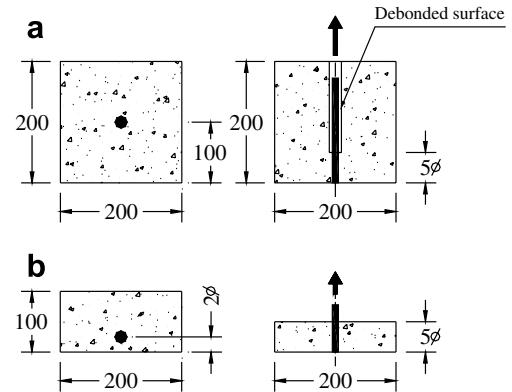


Fig. 8. Concrete cubes and the configuration of the specimens: (a) standard pull-out tests, (b) splitting pull-out tests.

where $\delta_1, \delta_2, \delta_3$ = slip measurements of the three LVDTs; l_a is the unloaded length (see Fig. 7); F is the applied pull-out load; E represents the elastic modulus of the bar; and A is the cross-sectional area of the bar.

The value of nominal bond stress was calculated as the recorded pull-out resistance force on the bar divided by the nominal surface area of the embedment length of the bar with the assumption of uniform bond stress distribution along the embedded length, as shown in Eq. (11). In all cases, pull-out failure (F) was defined as the point of maximum pull-out load

$$\tau = \frac{F}{CL} \quad (11)$$

where C is the circumference ($C = \pi d$ for round bars, $C = 4d$ for square bar), d is the diameter and L is the bonded length of the bar.

5.4. Splitting pull-out test

The splitting test is designed to give a more representative measure of the bond strength when a bar, such

as the ones shown in Fig. 8, is near the boundary. In order to investigate the splitting behaviour of reinforcing bars in GFRC concrete, 18 further pull-out specimens were tested with the bar placed eccentrically following the same test procedure as for the pull-out test. The configuration of the specimens is shown in Fig. 8. In the splitting test, the load and displacement values were used to calculate the corresponding nominal bond stress and slip in exactly the same way as for the standard pull-out test.

6. Experimental results

A summary of all the test results is presented in Table 2. From the standard deviation values it is apparent that there is considerable variability in the test results, in particular for δ_{peak} .

6.1. Slip characteristics

Typical slip characteristic curves can be seen in Fig. 9a, for the standard pull-out test, and Fig. 9b, for the splitting test which show results for the average slip of the loaded end and the slip of the free end. In the standard pull-out tests slip at the loaded end starts at a very early stage, but the free end only slips the maximum load, P_{max} . Hence, it appears that the debonding process is gradual, starting at the loaded end and spreading towards the free end. After initial free end slip, there is still additional resistance up to P_{max} . Soon after P_{max} , the resin rich layer of the surface appears to fail abruptly and the bar pulls out by several millimetres. The bar then locks again and frictional resistance results in relatively good residual bond stress (around 43% of τ_{max}).

In the case of the splitting pull-out test, slip again begins at the loaded end. However, this time bond failure occurs as a result of concrete splitting, as shown by the crack width measurements in Fig. 9b (curve 3). The maximum bond stress is only about 27% of τ_{max} . This value depends not only on the depth of the cover, but also on the bar surface and concrete cover characteristics.

6.2. Comparison between GFRC and plain concrete with embedded FRP reinforcement

Representative bond stress–slip curves for 8 mm GFRP bars in GFRC and concrete are shown in Fig. 10. The results show that the bond strength of the GFRP reinforcing bar to GFRC is approximately 1.6 times that of plain concrete. As seen in Fig. 10a and b the overall bond–slip characteristics of the GFRP bars in plain concrete and GFRC are similar. However, GFRC not only gives higher initial strength but also higher residual strength. The splitting bond stress is also about 26% higher in GFRC than in concrete, although the failure mechanism is the same.

Table 2
Summary of the tests results

Group	Specimen notations	Measured maximum load, $P_{\text{max_average}}$ (kN)	Bond strength, $\tau_{\text{max_average}}$ (MPa)	Standard deviation, σ_{τ} (MPa)	Slip at $P_{\text{max}}, \delta_{\text{peak_average}}$ (mm)	Standard deviation, σ_{δ} (mm)	Crack width at 85% of $P_{\text{max}}, w_{\text{max_average}}$ (mm)
I	M1P6	15.9	28.2	1.14	2.99	2.26	—
II	M0P6	36.8	16.3	—	1.44	—	—
III	M1P8	18.2	14.2	1.38	1.40	0.11	—
IV	M0P8	10.8	8.5	—	0.82	—	—
V	M1S6	4.3	7.7	2.16	0.41	0.07	0.005
VI	M0S6	8.1	3.6	—	0.08	—	0.500
VII	M1S8	5.0	3.9	0.46	0.88	0.17	0.004
VIII	M0S8	4.0	3.1	—	0.03	—	0.027
IX	M2P6	14.0	24.8	3.39	2.23	1.91	—
X	M2P8	14.1	11.0	1.09	0.72	0.64	—
XI	M2S6	2.8	4.9	0.84	0.48	0.12	0.001
XII	M2S8	4.9	3.8	1.30	0.25	0.06	0.001

Notes

M1 P 6
 M0 P 6
 M1 S 6
 M0 S 6
 M2 P 6
 M2 P 8
 M2 S 6
 M2 S 8

6 = 6mm diameter steel rebar
 8 = 8mm square GFRP rebar

P = Pull-out
 S = Splitting

M0 = Plain concrete
 M1 = Mix Design 1 (fibre = 2%)
 M2 = Mix Design 2 (fibre = 3%)

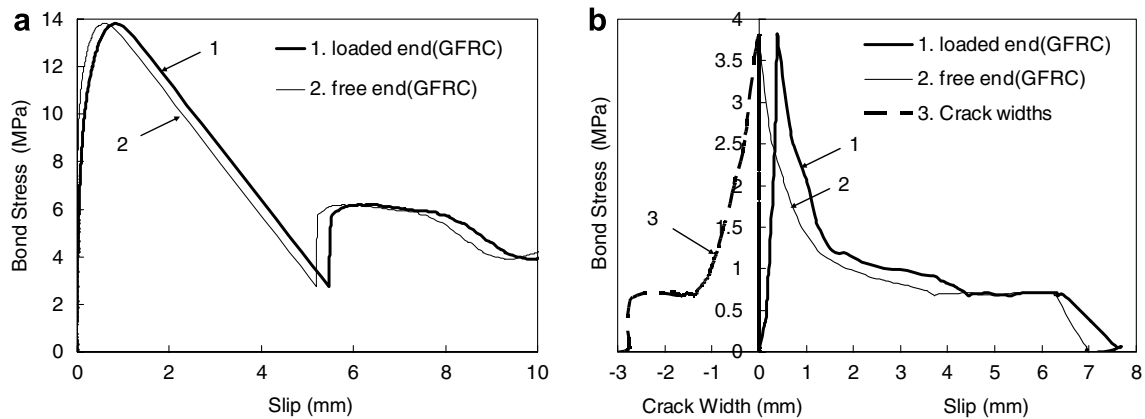


Fig. 9. Bond stress-slip response (8 mm GFRP bar).

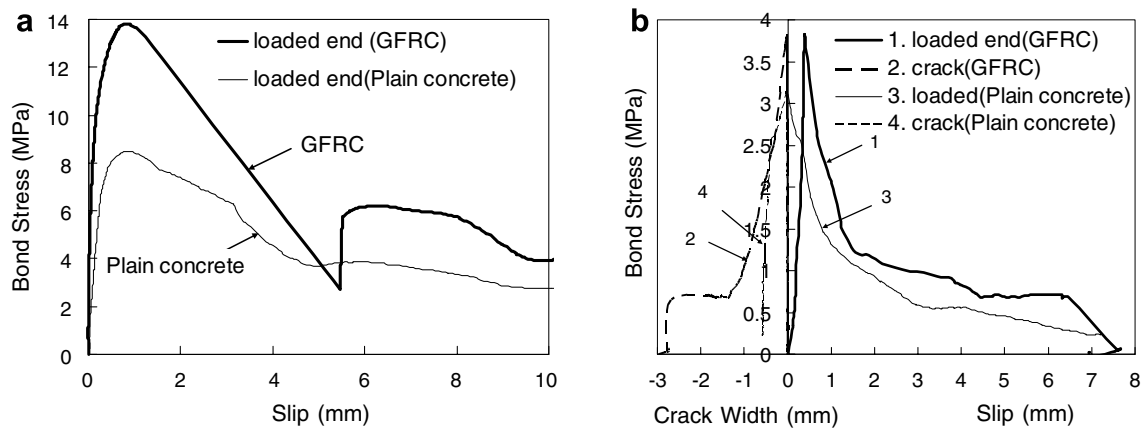


Fig. 10. Bond stress-slip response in GFRC in GFRC and concrete (8 mm GFRP bar).

6.3. Comparison of steel and GFRP bar

From Fig. 11a and b, it can be seen that steel reinforcement achieves much higher pull-out and splitting strengths than the FRP bars. This may be partly attributed to the fact that the steel bar diameter is smaller, having only 44% of the area of the FRP bar and the steel bar has much larger surface deformations. However, from Fig. 11a, it can be seen that the failure development is somewhat different from that for FRP, since slippage in steel occurs suddenly at P_{\max} and most likely without any damage to the bar surface.

6.4. Comparison of Mix 1 and Mix 2

Fig. 12a–d show the results of bond stress versus slip for 6mm steel and 8 mm GFRP bars for two different mixes of GFRC. In the standard pull-out tests, the bond strength for Mix 1 with the lower amount of fibre reinforcement is higher than for Mix 2 both for steel and FRP, but with very similar overall characteristics. It appears that the higher compressive and tensile strength associated with Mix 1 is due to its greater age at the time of testing and is more

important than the lower percentage of glass fibre it contained. In addition, the positive effect of increase in fibre volume in Mix 2 may have been diminished by increased air entrapment.

From the bond tests it can be concluded that, due to improved bond characteristics in GFRC (over normal concrete), it is possible to design FRP GFRC elements with reduced cover requirements since FRP reinforcement does not corrode. Now that this has been established, thin GFRC elements with FRP reinforcement will be examined further in the following section.

7. Analysis of FRP reinforced GFRC

To enable direct comparisons to be made with the work on GFRC cross-sections presented earlier, the same basic dimensions of the elements have been adopted here. This means that the overall depth of the unit has been kept at 110 mm and the thickness of the GFRC generally maintained at 10 mm. A cover of 10 mm all around the FRP bar has also been assumed. The FRP bar used as reinforcement is an 8 mm square GFRP bar having elastic modulus $E = 41$ GPa and strength around 900 MPa. Typical

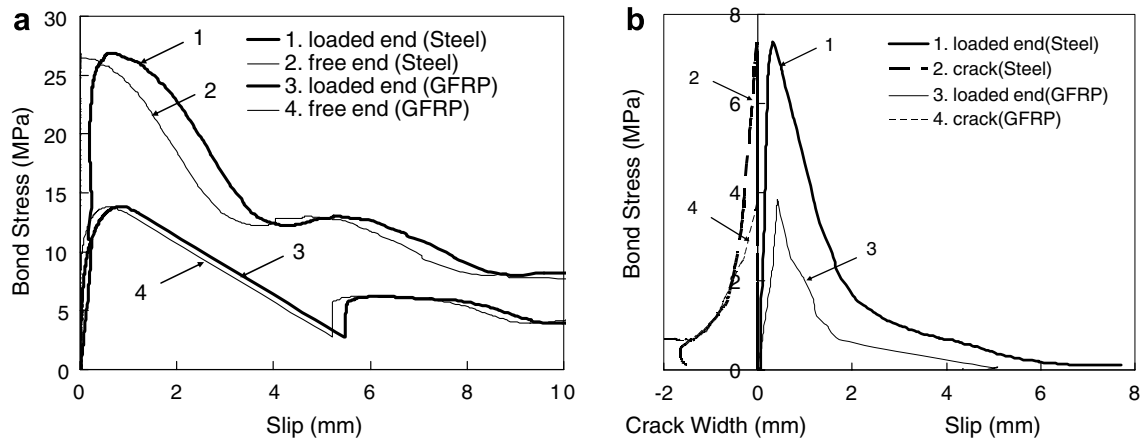


Fig. 11. Pull-out stress and slip response (comparison of steel and GFRP).

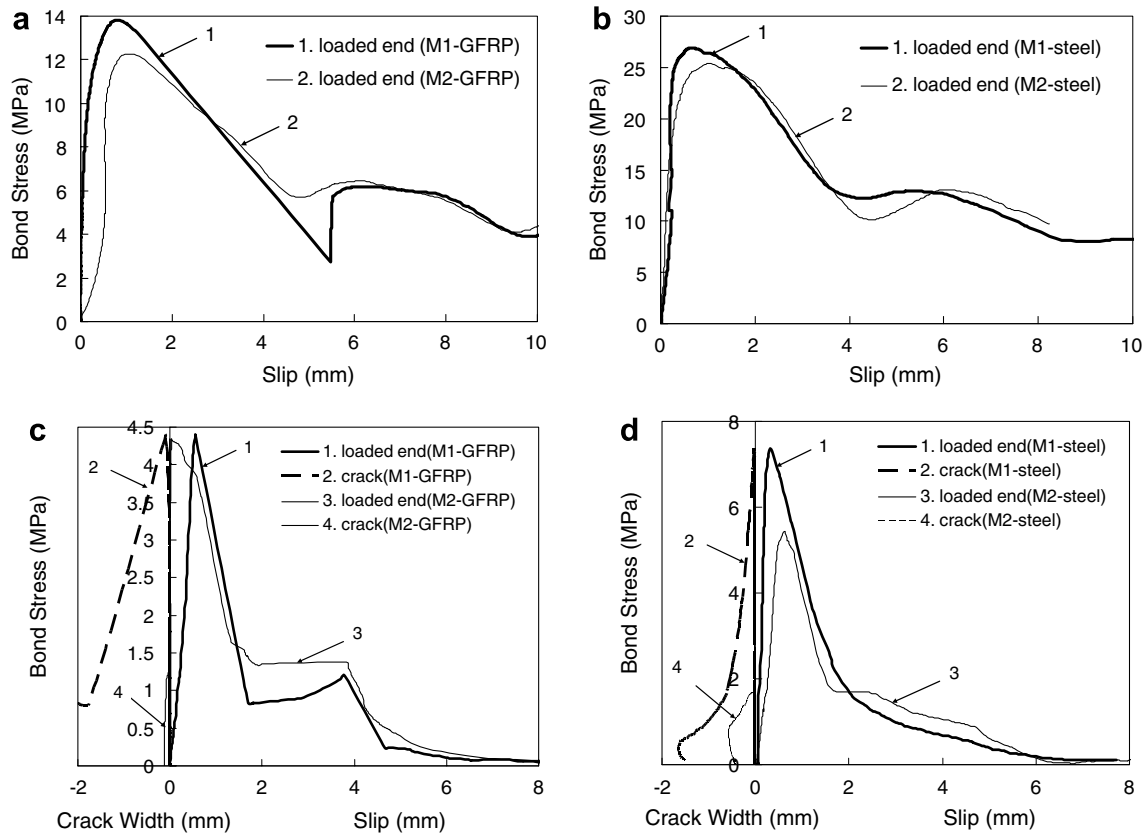


Fig. 12. Pull-out stress and slip response (comparison of Mix 1 and Mix 2 with 6 mm steel bar and 8 mm GFRP bar).

cross-sections for section types M13 and M5, taken from Kim et al. [8], are shown in Fig. 13.

7.1. Flexural capacity, deflection and crack widths

To simplify the problem, the following are some of the assumptions adopted for the purposes of this section analysis.

1. Plane sections remain plane after bending, i.e. a linear strain distribution is assumed through the cross-section.
2. There is perfect bond between the GFRC and the reinforcing FRP bars.
3. No tensile stress is carried by the concrete below the neutral axis.
4. GFRC behaves in compression like conventionally reinforced concrete.

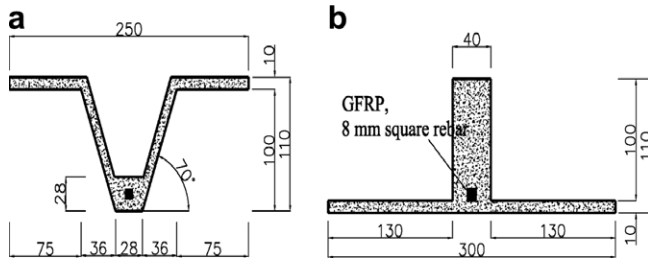


Fig. 13. Typical FRP reinforced GFRC section: (a) Type M13, (b) Type M5.

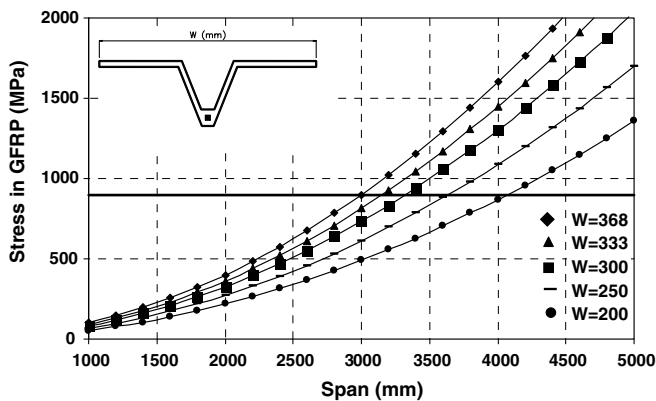


Fig. 14. Stress in GFRP (Type M13 – reinforced).

The dead (D) and live (L) ultimate load combination used in BS8110 [11] is $1.4D + 1.6L$. This leads to a design ultimate load of 10.8 kN/m^2 which has been used to calculate the corresponding stress in the GFRP bar. Figs. 14 and 16 compare the stress in the GFRP rebar for different span lengths and for various element widths (W) ranging from 200 to 368 mm and 120 to 360 mm, for section type M13 and M5, respectively. In terms of capacity, the maximum span length for such permanent formwork is shown to reach nearly 4 m. As can be seen from Fig. 15 dealing with

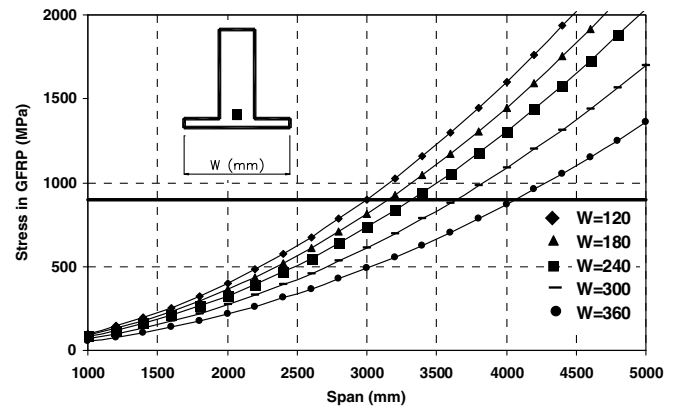


Fig. 16. Stress in GFRP (Type M5 – reinforced).

normalised deflection and capacity, for a similar unreinforced section (in case of $W = 250 \text{ mm}$, section type M13) with GFRC strength of 6 MPa, the maximum span length is just over 1 m. On the other hand, for section type M5 in Fig. 17 ($W = 300 \text{ mm}$), the span lengths of up to 3 m can be achieved.

Though the increase in capacity due to the addition of GFRP reinforcement is spectacular, deflections and crack widths need to be examined as well. At the moment there are no design recommendations for GFRC reinforced with FRP so the recommendations by ACI committee 440 [9] for FRP reinforced concrete have been used. As far as deflections and cracking are concerned the ACI proposes the following Eqs. (12)–(14) for deflection, δ , effective moment of inertia of cracked section, $I_{cr,e}$, and crack widths of FRP reinforced members, ω , respectively

$$\delta = \frac{5wL^4}{384EI} \text{ for UDL or } \frac{Ps}{48EI}(3L^2 - 4s^2) \text{ for four point load} \quad (12)$$

where w is the distributed load, P is the total service concentrated load divided into two concentrated loads $P/2$ each applied at a distance s from the support, and L , E

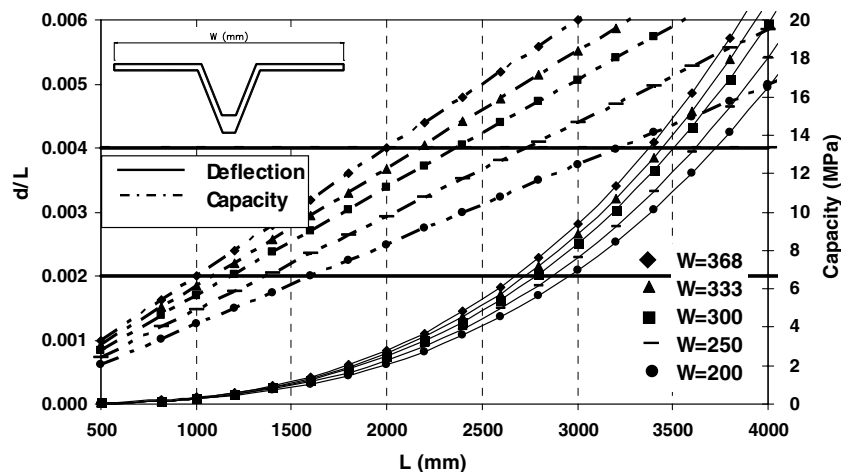


Fig. 15. Deflection and capacity (Type M13 – unreinforced).

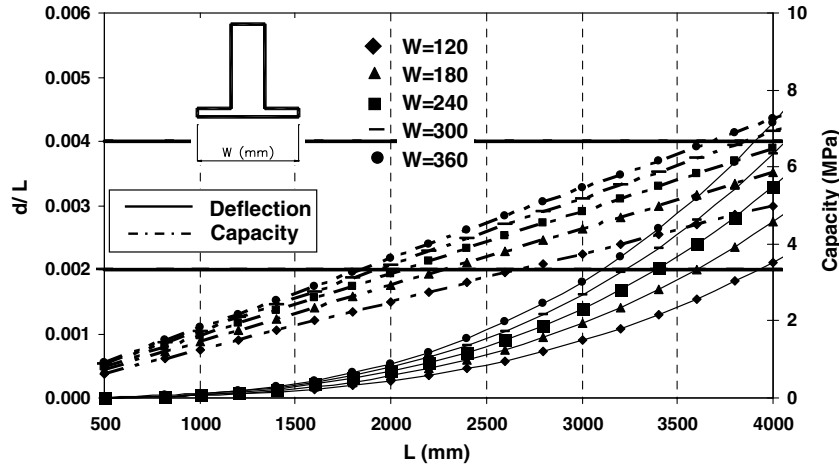


Fig. 17. Deflection and capacity (Type M5 – unreinforced).

and I are the span length, elastic modulus and second moment of inertia of the bar, respectively

$$I_{cr,e} = \left(\frac{M_{cr}}{M_a} \right)^3 \beta_d I_g + \left[1 - \left(\frac{M_{cr}}{M_a} \right)^3 \right] I_{cr} \leq I_g \quad (13)$$

where M_{cr} is the cracking moment, M_a is the applied moment and Reduction coefficient, $\beta_d = \alpha_b \left[\frac{E_f}{E_s} + 1 \right]$, (α_b = bond-dependent coefficient; E_f , E_s = modulus of elasticity of fiber and steel, respectively), and I_g is the gross moment of inertia, and I_{cr} is the moment of inertia of transformed cracked section

$$\omega = \frac{2.2}{E_f} \beta k_b f_f \sqrt[3]{d_c A} \quad (14)$$

where β is the ratio of the distance from the neutral axis to the extreme tension fibre to the distance from the neutral axis to the centre of the tensile reinforcement, k_b is the bond-dependent coefficient, f_f is the stress in the FRP reinforcement in tension, d_c is the thickness of the concrete cover measured from extreme tension fibre to the centre of the bar, and A is the effective tension area of concrete, defined as the area of concrete having the same centroid as that of tensile reinforcement, divided by the number of bars.

Eq. (13) is only valid for $M_a > M_{cr}$. The factors α_b and k_b are intended to reflect the weaker bond characteristics of some FRP bars. However, from previous work at Sheffield University [12,13], the authors consider that these factors are unnecessary for FRP bars. The modified equations were used to determine the deflections and crack widths for the FRP reinforced GFRC section shown in Fig. 18. It is evident, that even though the capacity of this section is adequate for spans of up to 4 m, at that span it would exceed both the deflection and crack width limits. In fact, type M13 section is only capable of spanning 2.60 m before the crack width limit of 0.5 mm is exceeded and 2.60 m before it exceeds the deflection limit of $L/250$. For type M5 section, the maximum span is just 2.55 m and 2.7 m in terms of the crack width and deflection limits,

respectively. But, the latter section needs more concrete volume (5 times more) than type M13 and, hence, is less economic.

There are three main options for increasing the performance of the section with regard to deflection and crack width

- decrease the strain in the FRP bar by increasing the amount of reinforcement,
- increase the depth of the cross-section,
- provide an intermediate support.

7.2. Shear capacity

To predict the shear capacity, ACI Committee 440 [9] Eq. (15) and RILEM TC 162 [14] Eqs. (16)–(19) are used.

$$V_c = \frac{\rho_f E_f}{90 \beta_1 f'_c} \left(\frac{\sqrt{f'_c} b_w d}{6} \right) \quad (15)$$

where ρ_f = flexural reinforcement ratio, E_f = modulus of elasticity of the FRP, β_1 = factor for concrete strength, f'_c = compressive strength of concrete, b_w = width of the web, and d = distance from extreme compression fibre to centroid of tension reinforcement

$$V_c = V_{cd} + V_{fd} + V_{wd} \quad (16)$$

$$V_{cd} = [0.12k(100\rho_1 f_{ck})^{1/3} + 0.15\sigma_{cp}] \cdot b_w d \quad (17)$$

where $k = 1 + \sqrt{\frac{200}{d}} \leq 2$, $\rho_1 = \frac{A_s}{b_w d} \leq 2\%$, A_s = area of tension reinforcement, b_w = minimum width of the section over the effective depth, $\sigma_{cp} = \frac{N_{sd}}{A_c}$, and N_{sd} = longitudinal force in section

$$V_{fd} = 0.7k_f k_l \tau_{fd} b_w d \quad (18)$$

where $k_f = 1 + n \left(\frac{h_f}{b_w} \right) \left(\frac{h_f}{d} \right) \leq 1.5$, h_f = height of the flanges, b_f = width of the flanges, b_w = width of the web, $n = \frac{b_f - b_w}{h_f} \leq 3$, $k_l = 1 + \sqrt{\frac{200}{d}} \leq 2$, and $\tau_{fd} = 0.12f_{RK,4}$

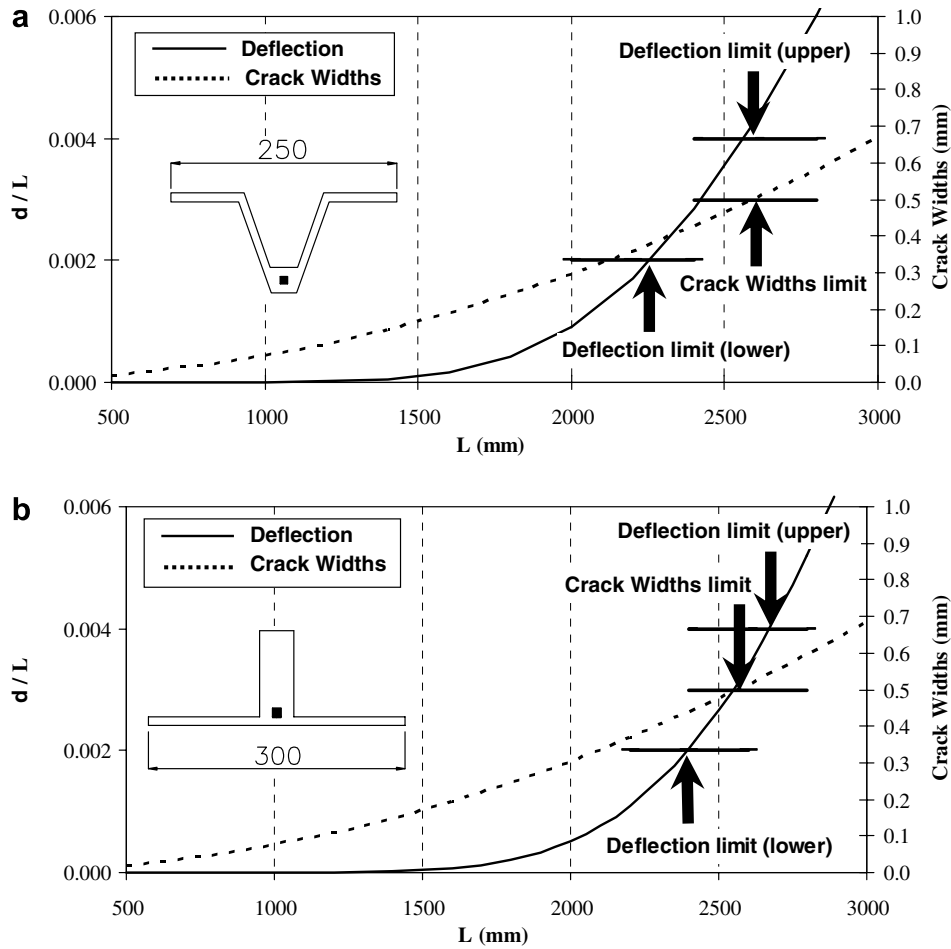


Fig. 18. Deflection and crack widths over typical FRP reinforced GFRC section: (a) Type M13, (b) Type M5.

$$V_{wd} = \frac{A_{sw}}{s} 0.9 d f_{ywd} (1 + \cot \alpha) \sin \alpha \quad (19)$$

where s = spacing between the shear reinforcement measured along the longitudinal axis, α = angle of the shear reinforcement with the longitudinal axis, and f_{ywd} = design yield strength of the shear reinforcement.

8. Overall system of FRP reinforced GFRC

8.1. Experimental analysis

To validate the design assumptions, two GFRC panels (Type M13) reinforced with GFRP were manufactured for experimental testing as shown in Fig. 19. These panels (L30G3, L30G2) were 3000 mm long and were provided with 8 mm square GFRP rebars and reinforced with 3% and 2% of chopped glass fibre, respectively. The concrete mix used in the analysis is given in Table 3. The average compressive strength of GFRC, obtained by testing 100 mm cubes to British Standard [15] at 28 days after casting, was 61.4 MPa and 69.8 MPa for L30G3, L30G2, respectively. The average splitting tensile strength of cylindrical specimens, determined by splitting tests on 150 mm

diameter \times 300 mm long cylinders to British Standard [16] at 28 days after casting, was 7.0 MPa and 6.2 MPa for L30G3, L30G2, respectively.

The panels were tested simply supported over a span of 2880 mm, and loaded by two concentrated line loads placed at equal distance from the support (960 mm for L30G3 and 740 mm for L30G2), as shown in Fig. 20. Displacement measurements were taken by LVDTs, at locations indicated in Fig. 20. The load was applied at a slow pace (initially 1 kN/min) by means of hydraulic jack in displacement control. Deflection and load values were monitored by means of a data acquisition system.

L30G3 was tested monotonically to failure. Failure occurred due to shear in the webs located in the shear span. The shear cracks were visible and opened widely before failure, hence though failure was abrupt it was not unexpected. After observing the fibre distribution along the failure surface of L30G3, it was noticed the direction of casting may have influenced the fibre orientation.

To amplify the shear load in the shear span, it was decided to reduce the shear span for L30G2. It was also decided to apply a load cycle just after cracking and a load cycle at 8 kN. The first load cycle was intended to provide an indication of damage at the load that the panel would

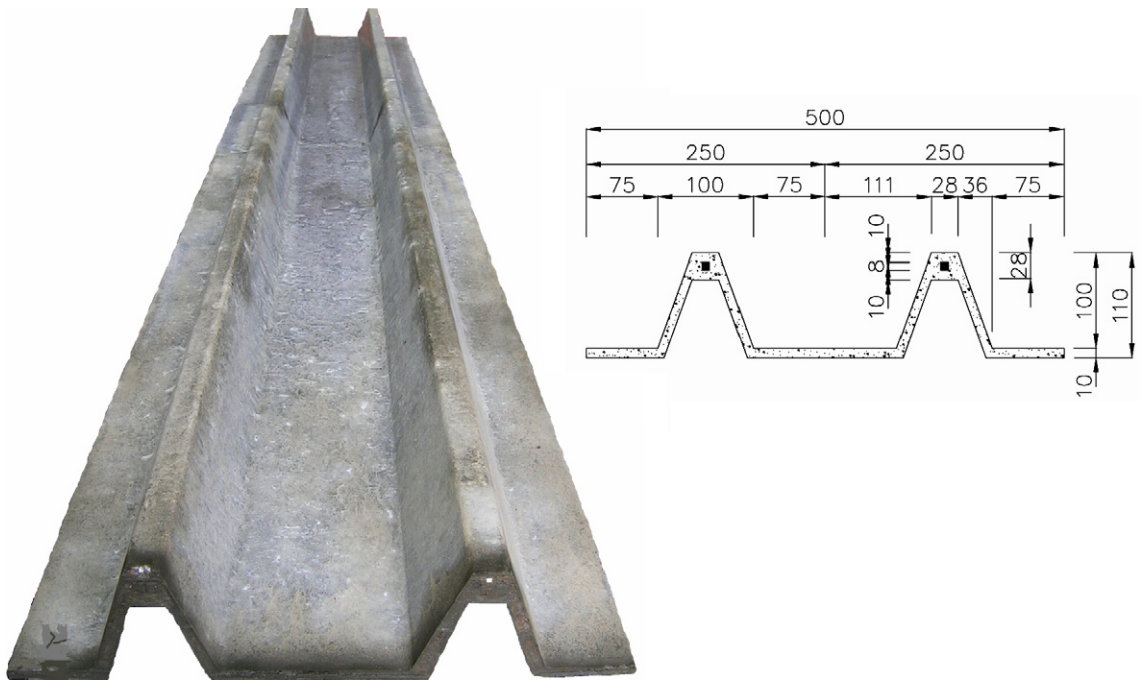


Fig. 19. Testing specimen.

Table 3
Proportions of GFRC mixtures in kg/m³

Mix code	Cement OPC	Fibre glass	Water	W/C	Aggregate sand (#2 sieve)	Super-plasticizer	Volume glass contents (%)	PFA
L30G3	52.5	3.15	19.71	0.375	52.5	1.21	3	21.0
L30G2	52.5	2.10	19.71	0.375	52.5	1.21	2	21.0

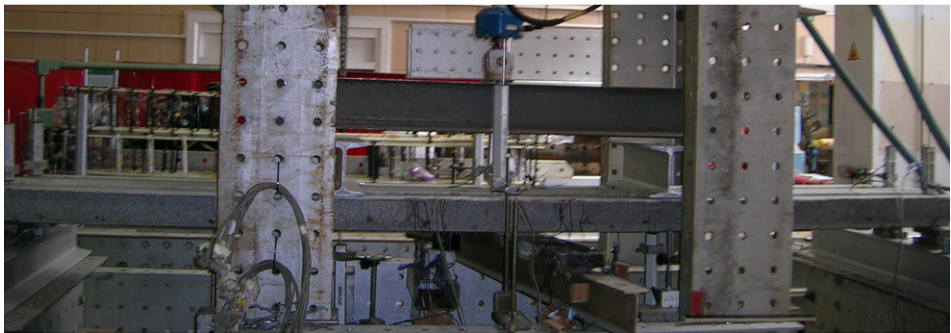
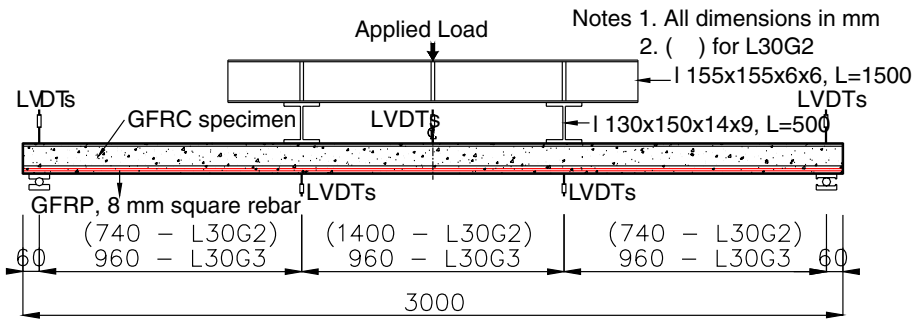


Fig. 20. Instrumentation and measurement points on panel L30G3 and L30G2.

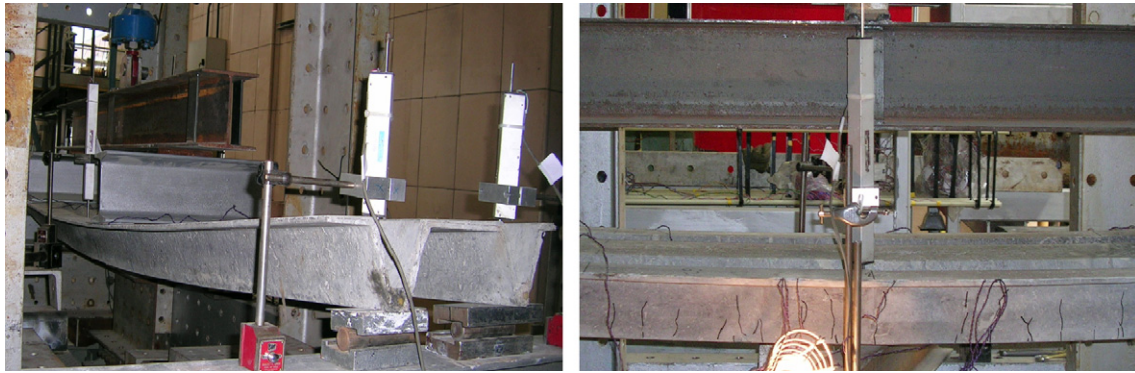


Fig. 21. After testing.

have failed if it had no FRP reinforcement. The second load cycle was intended to examine if shear cracks would propagate under repeated loading. Fig. 21 shows the large deflection achieved during loading as well as the cracks developed in the central region. Cracking started in the pure bending moment zone, but as the load was increased, shear stress induced inclined cracks led to failure.

8.2. Discussion of results

(a) Load–deflection

The load–deflection curves for both specimens are shown in Fig. 22a. The figure also shows the load deflection curve predicted by the ACI 440 equation (13). The predicted curves are exceptionally good and demonstrate that the ACI deflection equations are also appropriate for thin GFRF reinforced FRP. To enable a better comparison between the two specimens, the moment resistance versus normalised deflection curves are shown in Fig. 22b. The deflections are normalised to eliminate the difference in the position of the load. As it can be seen, there are no major differences in the deflection response between L30G3 and L30G2 even though they have a different amount of glass fibre reinforcement. Furthermore, there was no evidence of bond slip between GFRF and GFRF which confirms that thin concrete elements can be achieved if concrete is reinforced with fibres.

(b) Flexural capacity

The flexural capacity of the panels can be estimated by using the ACI440 equation or simple section analysis (SA1). The predictions from these two approaches are shown in Table 4, together with the experimented results. It is evident that these approaches underestimate the flexural capacity. Hence, a more sophisticated section analysis was undertaken, first by taking into account the stress–strain characteristics for GFRF in compression as measured from experiments (SA2) and by using the stress–strain potential in the tensile region of GFRF (SA3). The results from these analyses are also shown in Table 4. Since the specimens failed in shear, it can be assumed that their full flexural capacity is higher than achieved experimentally. That means that only SA3 pre-

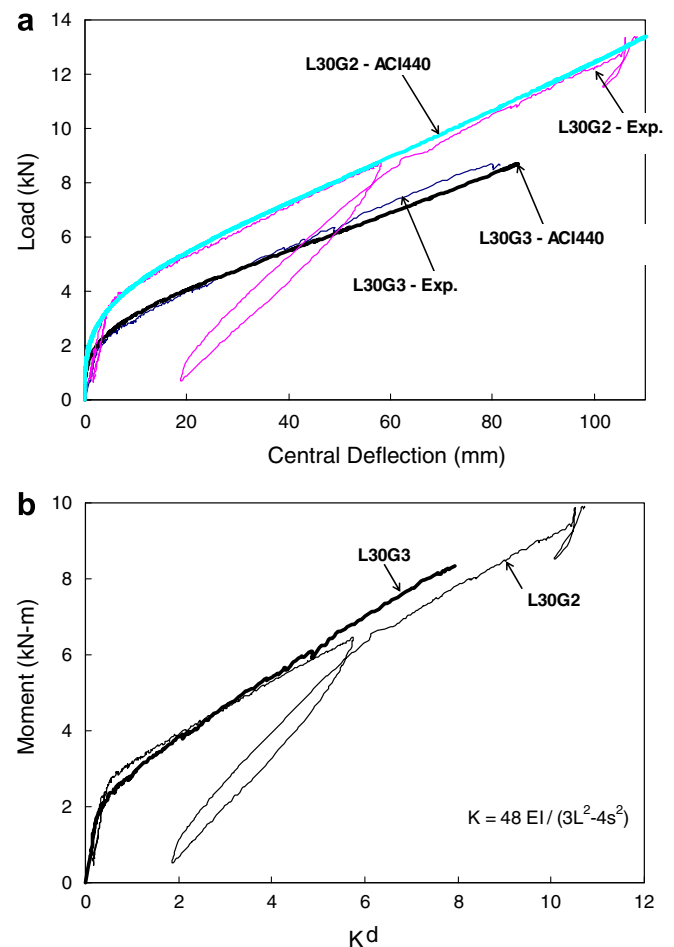


Fig. 22. The average measured load–deflection and moment resist relationships for L30G3 and L30G2: (a) load–deflection, (b) moment resistance.

dicts the capacity adequately. To confirm the validity of this analysis, the strains in the flexural reinforcement at the failure load obtained in the experiments was calculated and is shown in the table in parentheses. These predictions are close to the experimental values, and hence confirm that this type of analysis is appropriate for FRP reinforced GFRF.

Table 4
Measured and calculated ultimate load and strain in reinforcement

	Ultimate load, P_n (kN)					Strain in reinforcement (mm)			
	Exp.	ACI 440	SA1	SA2	SA3	Exp.	SA1	SA2	SA3
L30G3	8.7	8.3	8.4	9.2	10.3	0.0103	0.0146	0.0159	0.0136 (0.0107)
L30G2	13.4	11.0	11.9	13.3	14.7	0.0112	0.0156	0.0176	0.0153 (0.0133)

Notes: SA1 – Concrete no tension, SA2 – GFRC no tension, SA3 – GFRC with tension.

Table 5
Measured and calculated shear capacity

Exp.	ACI 440				RILEM TC162			
	(web only)		(transformed)		(web only)		(transformed)	
	Con.	Fibre	Con.	Fibre	Con.	Fibre	Con.	Fibre
L30G3	4.3	0.8	1.6	1.8	0.6	2.6	1.2	1.2
L30G2	6.7	0.7	1.5	2.0	0.6	2.8	1.2	1.2

(c) Shear capacity

The determination of the shear capacity of thin concrete sections is not easy since there are no codes of practice or recommendations dealing with such elements. Hence the shear capacity is predicted by first assuming that only the web is effective in resisting shear (web only) and then an equivalent rectangular section is considered (transformed). Initially, the ACI 440 equation (15) for FRP RC are used as shown in Table 5, but the results are very conservative. Then Eqs. (16)–(19) for GFRC proposed by RILEM TC 162 [14] are used. Here, the equations are modified to account for the FRP reinforcement by multiplying the reinforcement ratio by E_{FRP}/E_{steel} . This approach is used extensively in European recommendations for FRP RC design guidelines – European Committee for Standardization [17] and Institution of Structural Engineers [18]. The RILEM approach appears to be more suitable for thin FRP reinforced GFRC, even though the results are still very conservative for the case of L30G3. It should be noted that L30G3 failed due a horizontal crack developing just above the flexural reinforcement in the web. This mode of failure is not usually found in RC elements and may require a more direct check in thin GFRC elements.

9. Conclusions

Pull-out tests showed that the bond between the GFRP reinforcement and GFRC was approximately 60% greater than that for GFRP reinforcing bars embedded in plain concrete.

Equations for the optimum design of uniform thickness GFRC sections have been developed for use of these sections as permanent formwork.

FRP reinforced GFRC sections have a higher capacity than GFRC sections, but unpropped span lengths are restricted by the occurrence of large deflections and crack widths.

In order to predict the actual service load deflection based on the experimental results, simple empirical meth-

ods such as using the modified ACI 440 code were shown to be very accurate.

In terms of capacity, FRP/GFRC thin structural elements can be designed using a sophisticated section analysis (SA3) that considers the stress–strain characteristics of GFRC in tension and compression. In terms of shear capacity, the RILEM recommendation, modified to account for FRP, is shown to offer the least conservative estimate of resistance, but further research is required to determine the web shear resistance.

References

- [1] Pilakoutas K, Petkovski M. The development of the decathlon drainage channels. In: Proceedings of the 12th international congress or the international glassfibre reinforced concrete association, Dublin, 2001. p. 3–11.
- [2] Rockey KC, Evans HR. The behaviour of corrugated flooring systems. In: Thin walled steel structures – their design and use in buildings, Symposium at University College of Swansea, September 1969; 11–14. p. 236–57.
- [3] Timoshenko SP. Theory of plates and shells. McGraw-Hill; 1959.
- [4] Hopkins RB. Design analysis of shafts and beams. McGraw-Hill; 1970.
- [5] Lee CL, Mioduchowski A, Faulkner MG. Optimization of corrugated claddings. J Struct Eng 1995(August):1190–6.
- [6] Chung KF. The state-of-the-art of section property calculation of structural members with arbitrary shape. J Construct Steel Res 1995;32:127–41.
- [7] Rajendran SA. Fortran program for computing the geometric properties of plane lamina and axi-symmetric bodies. Comput Struct 1995;54(5):859–63.
- [8] Kim GB, Waldron P, Pilakoutas K. Applications of FRP/GRC in permanent formwork. In: La Tegola A, Nanni A, editors. Proceedings of the first international conference on innovative materials and technologies for construction and restoration, Lecce, Italy, June 6–9, vol. 1. Linguori Editore; 2004. p. 589–600. ISBN: 88-207-3678-8.
- [9] ACI 440.1R-01. Guide for the design and construction of concrete reinforced with FRP bars. American Concrete Institute, Farmington Hills, Michigan, 2001.
- [10] iRRT. International Round Robin Test for FRP reinforcement. <<http://www.shef.ac.uk/~tmrnet/rrt>>, Sheffield, 2002.
- [11] British Standards Institution, BS8110. Part 1: Code of practice for design and construction. British Standards Institution, London, 1997.

- [12] Sooriyaarachchi H. Tension stiffening effect in GFRP reinforced concrete elements. PhD thesis, Dept of Civil and Structural Eng, The University of Sheffield, 2006.
- [13] Al-Sunna RAS. Deflection behaviour of FRP reinforced concrete flexural members. PhD thesis, Dept of Civil and Structural Eng, The University of Sheffield, 2006.
- [14] RILEM TC 162-TDF. Test and design methods for steel fibre reinforced concrete, s-e design method; final recommendation, *Materials and structures*, vol. 36, October 2003. p. 560–7.
- [15] British Standards Institution, BS1881-116. Part 116: Method for determination of compressive strength of concrete cubes. British Standards Institution, London, 1983.
- [16] British Standards Institution, BS1881-117. Part 117: Method for determination of tensile splitting strength. British Standards Institution, London, 1983.
- [17] European Committee for Standardization. Eurocode 2: Design of concrete structures – Part 1: General rules and rules for buildings, prEN 1992-1 (1st draft), CEN, 1999.
- [18] Institution of Structural Engineers. Interim guidance on the design of reinforced concrete structures using fibre composite reinforcement. IStructE, SETO Ltd, London, 1999.